Proceedings of ISFOG 2025
5TH INTERNATIONAL SYMPOSIUM ON
FRONTIERS IN OFFSHORE GEOTECHNICS
Nantes, France | June 9-13 2025

ISBN 978-2-85782-758-0

Developing an integrated modelling approach for anchor-line system

W. Liu, Y. Tian*, M. Cassidy, Q. Yang
The University of Melbourne, Melbourne, Australia

**yinghui.tian@unimelb.edu.au (corresponding author)*

ABSTRACT: Offshore mooring systems are critical for station-keeping of floating structures and typically comprise mooring lines and anchors embedded in the seabed. Current design guidelines often simplify the analysis by treating the mooring line segments in water, the embedded anchors and chains as separate systems. While these simplifications can reduce computational complexity, they may overlook the coupled interactions between components, leading to inaccuracies in predicting the overall system behavior. This paper introduces an integrated modelling approach for analysing the anchor-line system, implemented within the finite element package, named as UoMMoor. The approach employs macroelement models to represent the interactions between the chain and surrounding soil, as well as the behavior of the embedded anchor. These macroelements encapsulate complex soil-structure interactions, allowing for computational efficiency while maintaining predictive accuracy. To validate the proposed method, a case study simulating the installation process of a drag embedment anchor is presented. The results highlight the method's capability to model complex anchor-soil and chain-soil interactions in three-dimensional space, offering a more comprehensive and realistic framework for designing offshore mooring systems in deep water.

Keywords: Integrated; Macroelement; Anchor chain; Mooring system

1 INTRODUCTION

Mooring systems are increaseingly becoming indispendsible to secure floating wind turbines. As shown in Figure 1, a mooring system comprises mooring lines (including the segment suspended in water and embedded in the seabed) and embedded anchors (such as drag anchors or plate anchors). For the segment of embedded mooring line, metallic chains are commonly adopted due to their advantages of heavier weight and higher abrasion resistance when compared with wire or synthetic fibre rope (Yen and Tofani, 1984).

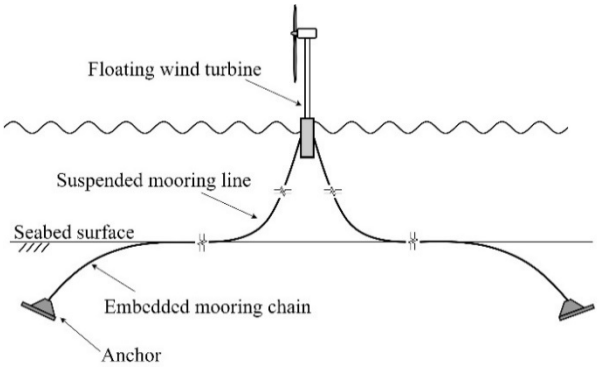

Figure 1. Illustration of a mooring system

In current design guidelines (ABS, 2017, 2022; DNV GL, 2017, 2018), the embeded anchors and chains in soil and the mooring line segments in water are analysed separately. For embedded anchors, the influcence of the mooring line segment in water is typically ignored, with a constant boundary condition (often a fixed chain inclination angle at the mudline) assumed (ABS, 2017; DNV GL, 2017). On the other hand, the mooring lines are assumed to be either fixed at the seabed or the embedded anchors are represented as simple springs on the seabed (ABS, 2022; DNV GL, 2018). These simplifications are inadequate to properly model the mooring system response (Wang et al., 2010), introducing uncertainty in design.

To achieve more realistic and accurate analyses, integrated modeling approaches that account for interactions between embedded anchors, chains in soil, and mooring lines in water are required. However, such studies are limited. Wung et al. (1995) modeled suspended and embedded chain segments using nonlinear truss elements, representing the anchor as a soil spring attached to the embedded chain end. Chain-soil interaction was captured using anchor-cable-soil elements derived from p-y and t-z curves commonly applied in pile analysis, while anchor-soil interaction was modeled using q-z curves. Wang et al. (2014)

developed a two-dimensional integrated model for drag embedment anchor installation. Their approach used a plasticity model (Aubeny and Chi, 2010) to describe anchor behavior, while the embedded chain configuration was governed by differential equations (Vivatrat et al., 1982). Tangential and normal soil resistances on the embedded chain segment were defined using empirical parameter-based equations.

This paper presents an integrated modelling approach, named as UoMMoor, based on a finite element framework for the analysis of anchor-line system in three-dimensional space. The soil resistances to a chain link are modelled by force-resultant model, which treats a chain link and its surrounding soil as macroelement by encapsulating the resultant soil resistance and the corresponding displacement of the chain link (Roscoe and Schofield, 1956; Tian and Cassidy, 2008). Similarly, anchor behaviour is described using a developed macroelement. A case study modelling the installation of a drag embedment anchor was conducted to demonstrate the capability and validity of the integrated modeling approach.

2 MACROELEMENT OF MOORING CHAINS

Liu et al. (2024a) proposed a macroelement to describe the soil resistances to embedded chain links in three-dimensional space. The soil resistances to the chain link are described by three components: T along the axial direction v, N along the normal direction w, and S along the lateral direction u, which are orthogonal to each other, as shown in Figure 2. The macroelement encapsulates combined soil resistance (T, N, S) with a yield surface, as shown in Figure 3. By properly modelling the intricate geometry of chain links, Liu et al. (2024b, c) carried out a large number of three-dimensional finite element analyses. By fitting the finite element results, Liu et al. (2024b) proposed the soil resistance yield surface equation for chain links:

$$f = \left(\frac{|N_t|}{N_{t\max}}\right)^t + \left[\left(\frac{|N_n|}{N_{n\max}}\right)^n + \left(\frac{|N_s|}{N_{s\max}}\right)^s\right]^{\frac{1}{p}} - 1 = 0 \quad (1)$$

where $N_t = T/A_n s_u$, $N_n = N/A_n s_u$ and $N_s = S/A_n s_u$ represent the dimensionless axial, normal and lateral soil resistances, respectively, and $N_{t\max} = T_{\max}/A_n s_u$, $N_{n\max} = N_{\max}/A_n s_u$ and $N_{s\max} = S_{\max}/A_n s_u$ are the corresponding uniaxial bearing capacity factors. Liu et al. (2024c) reported the values of uniaxial bearing capacity factors with respect to chain link type, embedment depth, link direction angle and interface condition. A_n is the project area of the chain link in u-v plane. s_u is the undrained shear strength of the soil. The parameters t, n, s, and p characterise the shape of the yield surface.

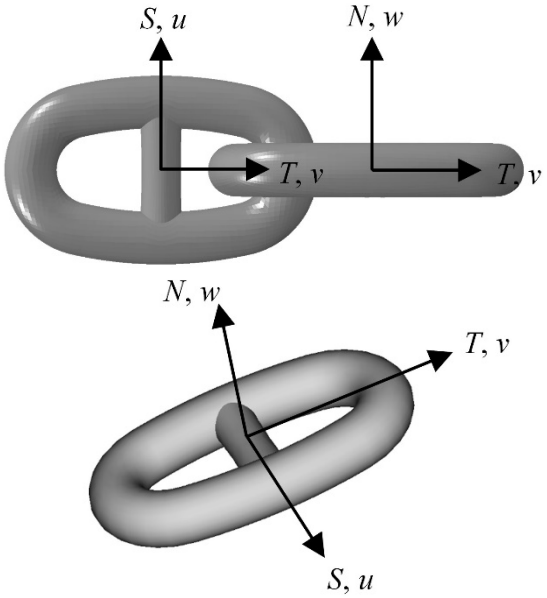

Figure 2. Soil resistances acting on chain links

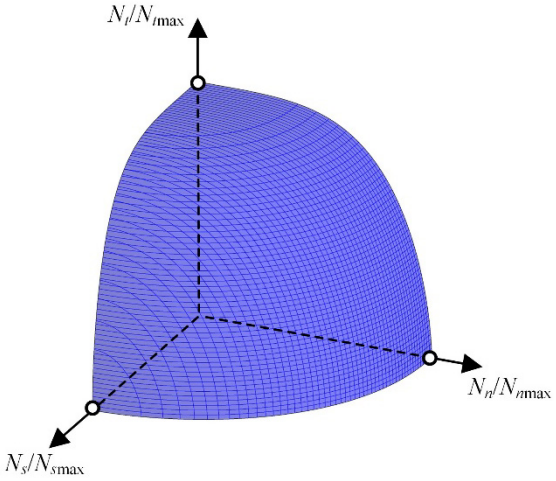

Figure 3. Soil resistance yield surface of chain link

The macroelement model for chain links assumes an associated flow rule, i.e. the plastic potential function g is same as yield surface function f. The incremental constitutive equation for the macroelement model is expressed as:

$$d\mathbf{N} = \mathbf{D}^e(d\mathbf{u} - d\mathbf{u}^p) = \mathbf{D}^{ep}d\mathbf{u} = \left(\mathbf{D}^e - \frac{\mathbf{D}^e\frac{\partial g}{\partial \mathbf{N}}\frac{\partial f}{\partial \mathbf{N}}^T\mathbf{D}^e}{H+\frac{\partial f}{\partial \mathbf{N}}^T\mathbf{D}^e\frac{\partial g}{\partial \mathbf{N}}}\right)d\mathbf{u} \quad (2)$$

where $d\mathbf{N}$ is the dimensionless soil resistance increment, $\mathbf{D}^e$ is the elastic stiffness matrix, $d\mathbf{u}$ is the

local displacement increment, $d\mathbf{u}^p$ is the local plastic displacement increment, $\mathbf{D}^{ep}$ is the elasto-plastic stiffness matrix, and H is a hardening item (see Liu et al. (2024a) for more details).

3 MACROELEMENT OF ANCHOR

Wang et al. (2022) proposed a macroelement model for plate anchors under six degree-of-freedom loads in three-dimensional space. As shown in Figure 4, the soil resistances to the plate anchor are denoted as a normal force N_{an}, two sliding forces S_2 and S_3, a torque T_{an} and two moments M_2, M_3, with corresponding displacements of u_{nan}, u_{s2}, u_{s3}, θ_{tan}, θ_{m2} and θ_{m3}, respectively. Wang et al. (2022) proposed the soil resistance yield surface equation for the plate anchor:

$$f = \left[\left(\frac{|N_{s2}|}{N_{s2\max}}\right)^{s_2} + \left(\frac{|N_{s3}|}{N_{s3\max}}\right)^{s_3} + \left(\frac{|N_{tan}|}{N_{tan\max}}\right)^{t_{an}}\right]^{\frac{1}{p_{an}}} + \left[\left(\frac{|N_{m2}|}{N_{m2\max}}\right)^{m_2} + \left(\frac{|N_{m3}|}{N_{m3\max}}\right)^{m_3} + \left(\frac{|N_{nan}|}{N_{nan\max}}\right)^{n_{an}}\right]^{\frac{1}{q_{an}}} - 1 = 0 \quad (3)$$

where $N_{nan\max}$, $N_{s2\max}$, $N_{s3\max}$, $N_{tan\max}$, $N_{m2\max}$ and $N_{m3\max}$ are the uniaxial bearing capacity factors, which are related to the aspect ratio of the plate. n_{an}, s_2, s_3, t_{an}, m_2, m_3, p_{an} and q_{an} are the parameters controlling the shape of the yield surface.

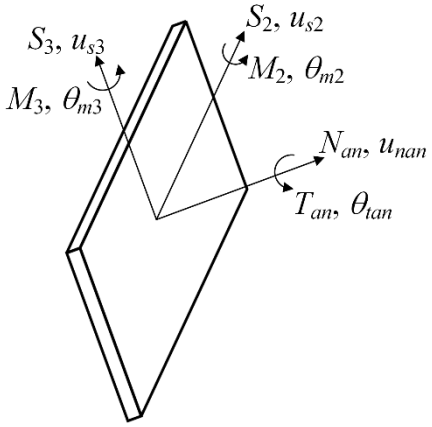

Figure 4. 6 degree-of-freedom soil resistances acting on plate anchor

4 IMPLEMENTATION INTO UOMMOOR

Liu et al. (2024a) proposed an approach based on a finite element framework for integrated modelling of anchor and mooring line system. The approach has been implemented into commercial software ABAQUS, while it is ready to be implemented into any other software packages for offshore floating system analysis. The macroelement of chain links and anchor were user-defined elements and coded via the user subroutine UEL (Dassault Systèmes, 2019). Liu et al. (2024a) proposed an efficient explicit integration algorithm to solve the incremental constitutive equations for the macroelements (see Liu et al. (2024a) for more details).

Figure 5 illustrates the components of the integrated mooring system model, where the chain elements are modelled using 3-node beam elements (B32H) and are connected using connector elements (UJOINT), which model relative rotation of adjacent chain links. The macroelement for a chain link is attached to the middle node of the chain element. The macroelement for the anchor is connected to the chain through a shank element. It is noted that this shank element only serves as a connection between the anchor macroelement and the chain in this integrated analysis, where the soil resistance to the shank is inherently accounted in the anchor macroelement model. Similarly, the fluke element acts as a visual indicator of the anchor position and inclination.

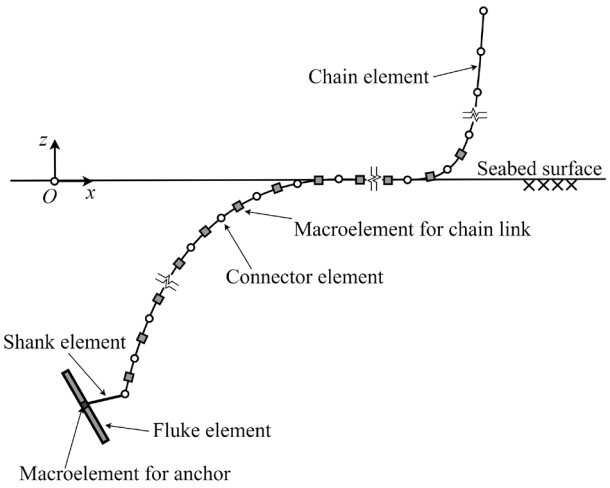

Figure 5. Illustration of integrated mooring system model

5 CASE STUDY

In this case study, the installation of drag embedment anchor was modelled using the integrated modeling approach. As shown in Figure 6, the anchor shank was initially located at the seabed surface and the attachment point (padeye) was at the origin of the global coordinate system. It is noted that the drag anchor is represented as a macroelement model by using the parameter of Wang et al. (2022) derived by 3D finite element analysis. The anchor line comprises a horizontal segment with a length of L_h = 200 m lying on the seabed surface and a vertical segment with a length of H_w = 100 m in water. The parameters for the

case study are summarised in Table 1. A common stud link chain with a bar diameter $d = 100$ mm is modelled, and the length of a chain element is adopted as $4d$, which is calculated by subtracting the overlap between chain links. The undrained shear strength of the seabed soil is $s_u = 5 + z_c$ kPa, where z_c is the embedment depth of the fluke centre. The drag embedment anchor was assumed to be installed in still water and the environmental loads from wave and current are neglected. The installation analysis is conducted by applying a horizontal displacement $U_x = 400$ m at the top end of the chain, which corresponds to the fairlead of an anchor handling vessel.

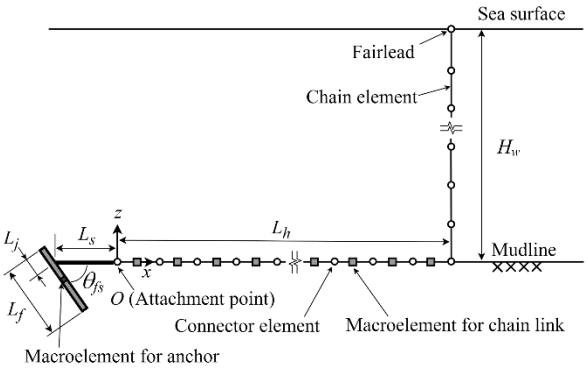

Figure 6. Illustration of integrated model for drag embedment anchor installation

Table 1. Parameters for case study

Type	Variable	Value
chain	Diameter, d (mm)	100
	Total length, L (m)	300
	Axial stiffness, EA (MN)	1005.3
	Air weight, W (kg/m)	219
Anchor	Fluke width, B (m)	3
	Fluke lengh, L_f (m)	2
	Distance from fluke edge to junction point, L_j (m)	0.5
	Fluke-shank angle, θ_f (°)	50
	Shank length, L_s (m)	3
Soil	Undrained shear strength at mudline, s_{um} (kPa)	5
	Shear strength gradient, k (kPa/m)	1
Water	Depth, z_w (m)	100

Figure 7 shows the variation of chain profiles with increasing U_x, as well as the anchor trajectory indicated by the attachment point and the fluke centre. With the anchor dipping into the seabed, an invert catenary chain profile can be observed in soil. When U_x was over ~170 m, the chain profile kept unchanged and the anchor reached an ultimate depth, where the attachment point and the fluke centre were 10.50 m and 12.75 m at depth, respectively.

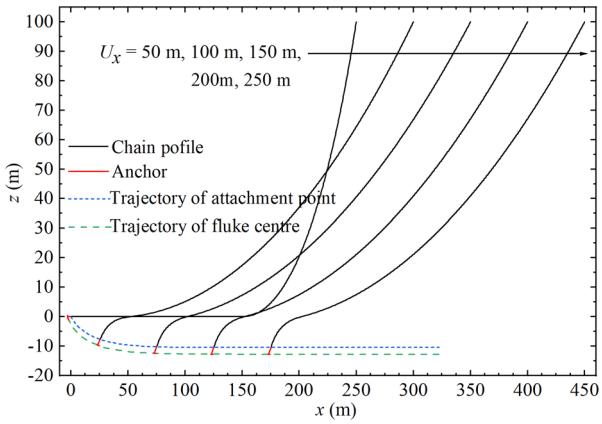

Figure 7. Chain profiles and anchor trajectory

Figure 8 shows the forces at the fairlead and the attachment point. When U_x was over ~170 m, the total force F at the fairlead and T_a at the attachment point reached steady values of 1005 KN and 611 kN, respectively, while the horizontal component F_x at the fairlead was 813 KN. At the ultimate state, the capacity from the anchor (T_a) contributed to 75% of the mooring force (horizontal force F_x).

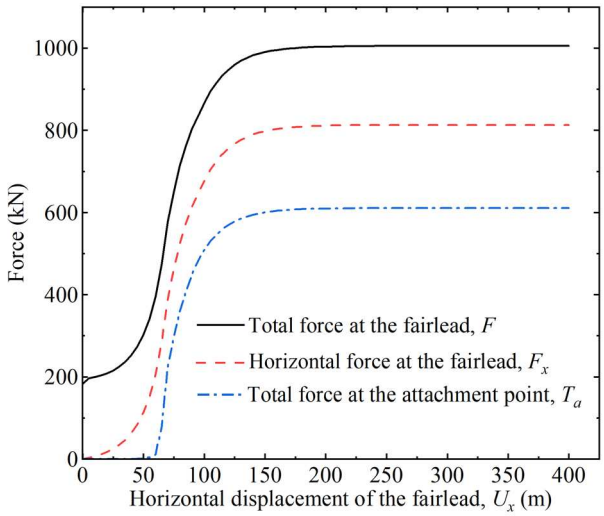

Figure 8. Force-displacement curves

Figure 9 shows the variation of the combined soil resistance to the anchor, which is called soil resistance path, during the anchor installation. At the ultimate embedment depth, the soil resistance path and its projection on $N_{nan}/N_{nan\max}$-$N_{s3}/N_{s3\max}$ plane reached the same point on the yield surface, which indicates the moment N_{m2} was zero and the anchor stopped rotating at this state.

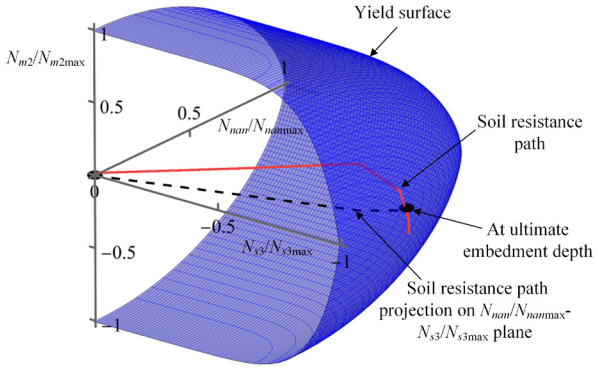

Figure 9. Normalised soil resistances to the anchor

Figure 10 shows the soil resistance to the chain links when U_x = 50 m, 100 m, and 250 m, respectively. Considering the alternate directions of the chain links, the chain links are divided into two groups based on the initial direction angle β_0, which is the angle between the *x*-*z* plane and local *w* axis of the chain link. Because the chain kept moving in the *x*-*z* plane, the combined soil resistance is (N_n, N_t) and (N_s, N_t) for the chain links with β_0 = 0° and 90°, respectively. When U_x = 50 m, the combined soil resistance to some of the chain links was within the yield surface for the chain links at the mudline (z/W = 0, where W = 3.6d is the link width), which means the soil resistance states of these chain links were in elastic stage. When U_x = 100 m or 250 m, the combined soil resistance to the chain links close to the attachment point was on the yield surface for deep embedded chain links ($z/W \geq 2.5$). In contrast, for the chain links close to the mudline, the combined soil resistance was also near the yield surface of z/W = 0, as the uniaxial bearing capacity factors decrease with decreasing depth.

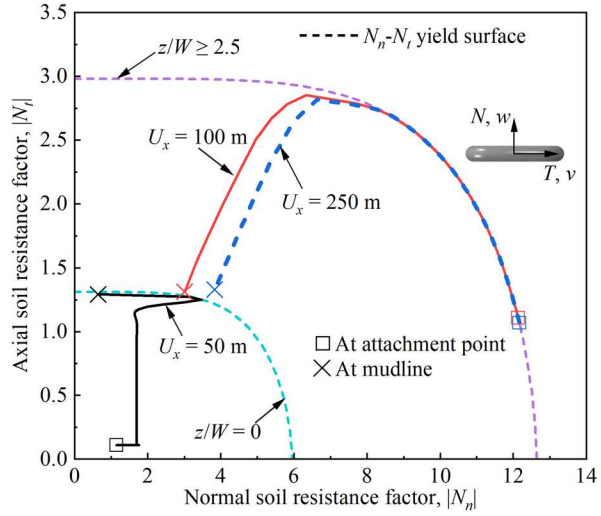

(a) dimensionless soil resistances to chain links with β_0 = 0°

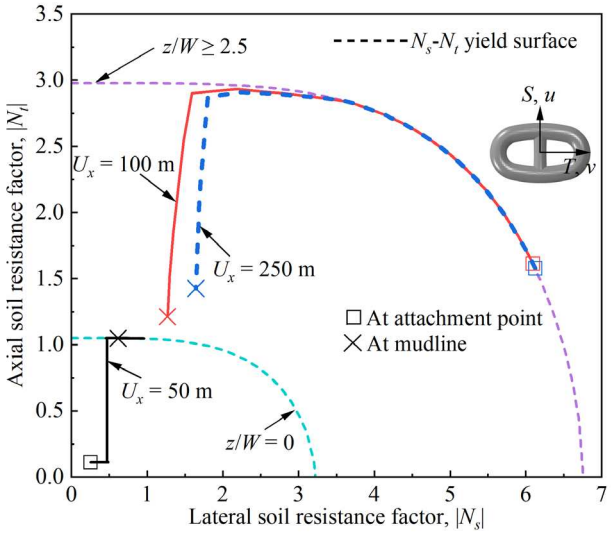

(b) dimensionless soil resistances to chain links with β_0 = 90°

Figure 10. Dimensionless soil resistances to chain links

6 CONCLUSIONS

This study presents the development of an integrated modelling approach for anchor-line system based on a finite element framework. This part of work aims to develop a modelling package that engineers can use for integrated anchor-mooring analysis, allowing implementation of different anchor and chain models with flexible and versatile interfaces. This approach takes advantage of macroelements to consider the chain-soil and anchor-soil interactions. Compared to the traditional finite element method, this integrated modeling approach utilises macroelements to avoid the need to model detailed continuum soil elements, thereby significantly enhancing computational efficiency. The advantages of this approach include: 1) the soil resistances to the chain and anchor are coupled, thereby enhancing the rigorousness and accuracy of the modelling; 2) this approach can be easily implemented into a structural analysis package with comparable complexity. The case study demonstrates the capability of the integrated modeling approach by modelling the installation process of a drag embedment anchor, where comparision with established studies, such finite difference methods of Degenkamp and Dutta (1989), was conducted in our jounral paper but not repeated here due to page limit.

AUTHOR CONTRIBUTION STATEMENT

Liu, W.: Methodology, Software, Formal Analysis, Visualization, Writing- Original draft. **Tian, Y.**: Conceptualization, Methodology, Supervision,

Writing- Reviewing and Editing, Funding acquisition. **Cassidy, M.**: Supervision, Writing- Reviewing and Editing. **Yang, Q.**: Writing- Reviewing and Editing

ACKNOWLEDGEMENTS

This research was supported though the corresponding author's Australian Research Council Future Fellowship (FT200100457).

REFERENCES

ABS (2017). Design and installation of drag anchors and plate anchors. American Bureau of Shipping, Houston, Texas.

ABS (2022). Guide for position mooring systems. American Bureau of Shipping, Spring, Texas.

Aubeny, C.P. and Chi, C. (2010). Mechanics of drag embedment anchors in a soft seabed. *Journal of Geotechnical and Geoenvironmental Engineering*, 136, 57–68.

Dassault Systèmes (2019). *SIMULIA user assistance 2019: Abaqus*. Dassault Systèmes Simulia Corp., Providence, Rhode Island.

Degenkamp, G. and Dutta, A. (1989). Soil resistances to embedded anchor chain in soft clay. *Journal of Geotechnical Engineering*. 115, 1420–1438.

DNV GL (2017). Design and installation of plate anchors in clay. DNVGL-RP-E302. Det Norske Veritas, Høvik, Norway.

DNV GL (2018). Position mooring. DNVGL-OS-E301. Det Norske Veritas, Høvik, Norway.

Liu, W., Tian, Y. and Cassidy, M.J. (2024a). A three-dimensional integrated modelling approach for anchor and mooring line system. (Ready to be submitted as a technical paper in 2025).

Liu, W., Tian, Y., Cassidy, M.J., O'Loughlin, C. and Watson, P. (2024b). A new analytical approach to model embedded anchor lines based on the yield surface of soil resistance. (Ready to be submitted as a technical paper in 2025).

Liu, W., Tian, Y., Cassidy, M.J., O'Loughlin, C. and Watson, P. (2024c). Numerical investigation of the capacity of anchor chain links in clay. *Journal of Geotechnical and Geoenvironmental Engineering*, 150(10): 04024090.

Roscoe, K.H. and Schofield, A.N. (1956). Stability of short pier foundations in sand. *British Welding Journal*, 3, 343–354.

Tian, Y. and Cassidy, M.J. (2008). Modeling of pipe-soil interaction and its application in numerical simulation. *International Journal of Geomechanics*, 8, 213–229. https://doi.org/10.1061/(ASCE)1532-3641(2008)8:4(213)

Vivatrat, V., Valent, P.J. and Ponterio, A.A. (1982). The influence of chain friction on anchor pile design. *Proceedings of the 14th Annual Offshore Technology Conference. Offshore Technology Conference*, Houston, Texas, pp. 153–163. https://doi.org/ 10.4043/4178-ms

Wang, J., Tian, Y., Liu, W. and Wang, L. (2022). Capacity envelope of plate anchors under six degree-of-freedom loads in clay. *Applied Ocean Research*, 126, 103267.

Wang, L.Z., Guo, Z. and Yuan, F. (2010). Quasi-static three-dimensional analysis of suction anchor mooring system. *Ocean Engineering*, 37, 1127–1138. https://doi.org/10.1016/j.oceaneng.2010.05.002

Wang, L.Z., Shen, K.M., Li, L.L. and Guo, Z. (2014). Integrated analysis of drag embedment anchor installation. *Ocean Engineering*, 88, 149–163. https://doi.org/10.1016/j.oceaneng.2014.06.028

Wung, C.C., Litton, R.W., Mitwally, H.M., Bang, S. and Taylor, R.J. (1995). Effect of soil on mooring system dynamics. *Proceedings of the 27th Annual Offshore Technology Conference*, Offshore Technology Conference, Houston, Texas, pp. 301–307. https://doi.org/10.4043/7672-ms

Yen, B.C. and Tofani G.D. (1984). Soil resistance to stud link chain. *Proceedings of the 16th Annual Offshore Technology Conference*, Offshore Technology Conference, Houston, Texas, pp. 479–488.